

# Polymer Chemistry

Accepted Manuscript



This is an *Accepted Manuscript*, which has been through the Royal Society of Chemistry peer review process and has been accepted for publication.

*Accepted Manuscripts* are published online shortly after acceptance, before technical editing, formatting and proof reading. Using this free service, authors can make their results available to the community, in citable form, before we publish the edited article. We will replace this *Accepted Manuscript* with the edited and formatted *Advance Article* as soon as it is available.

You can find more information about *Accepted Manuscripts* in the [Information for Authors](#).

Please note that technical editing may introduce minor changes to the text and/or graphics, which may alter content. The journal's standard [Terms & Conditions](#) and the [Ethical guidelines](#) still apply. In no event shall the Royal Society of Chemistry be held responsible for any errors or omissions in this *Accepted Manuscript* or any consequences arising from the use of any information it contains.

## ARTICAL

## Novel Phosphorus-Nitrogen-Silicon Flame Retardants and Their Application in Cycloaliphatic Epoxy Systems

Cite this: DOI: 10.1039/x0xx00000x

Pengjie Chao<sup>1</sup>, Yongjie Li<sup>2</sup>, Xiaoyu Gu<sup>3</sup>, Dandan Han<sup>2</sup>, Xiaoqin Jia<sup>2</sup>, Mengqiang Wang<sup>2</sup>, Tengfei Zhou<sup>2</sup> and Tao Wang<sup>\*1,2</sup>Received 00th January 2012,  
Accepted 00th January 2012

DOI: 10.1039/x0xx00000x

[www.rsc.org/](http://www.rsc.org/)

To solve the incompatibility of flame retardants with epoxy resin, two novel phosphorus–nitrogen–silicon flame retardants (DPP-Si and PSAP) containing active hydroxyl group were obtained via a simple and efficient synthesis. Both of the obtained flame retardants were characterized via FTIR, <sup>1</sup>H NMR, and <sup>31</sup>P NMR. Flame retardant epoxy composites (FR-Ep) were prepared with different contents of DPP-Si and PSAP in 3, 4-epoxycyclohexylmethyl-3, 4-epoxycyclohexane carboxylate (ERL4221), and cross-linked by UV-radiation and thermal curing. The influence of DPP-Si and PSAP on the flame-retardant properties of FR-Ep was investigated through limiting oxygen index (LOI) and vertical burning tests (UL-94) respectively, the results shows that the LOI of the FR-Ep containing 15 wt % of either DPP-Si or PSAP was about 27.6%, attained a V-1 rating, whereas pure epoxy resin has an LOI of 20.5%. The microstructures of the char were investigated by scanning electron microscopy (SEM), the SEM results indicated that the residual char of the FR-Eps after burning have compact and coherent appearance, which plays an important role in the excellent thermal stability and improves flame retardant of FR-Ep by means of isolating fire sources and cutting off from oxygen.

### Introduction

Demands to reduce fire hazards, which are common among highly combustible materials such as wood, plastics, and textiles, have gained high importance in recent years. The use of fireproof coatings in modifying these material surfaces is one of the most convenient, most economical, and most efficient ways to protect substrates against fire.<sup>1-3</sup> The advantage of fireproof coatings is that it allows the concentration of fireproof properties at the surface of the substrate, thereby preserving the bulk properties of the material.<sup>4-6</sup> Flame-retardant coatings can be applied in many fields, such as building construction, electrical applications, textiles, electronics, and transportation.<sup>7, 8</sup>

The common approach is the mechanical incorporation of flame retardant additives into the bulk polymeric matrix, which is mostly an inexpensive and fast-blending technique.<sup>9, 10</sup> For example, in the building and transportation industry, a popular way to impart flame retardant is by mixing its additives in paints and lacquers, which are used to coat surfaces.<sup>11, 12</sup> However, to be effective, the loading of flame retardant is usually too high, which significantly influences the strength and modulus elasticity of the materials.<sup>13, 14</sup> The way to reduce the flammability of a matrix is to chemically bind units to it by using flame retardant segments that contain functional groups.<sup>4,</sup>

<sup>15</sup> Through this approach, the flame retardant element becomes an integral part of the polymer chain and usually results in higher efficiency and longer durability of the FR effect.

The UV-curing technique is being increasingly used in industrial flame retardant coating applications.<sup>16, 17</sup> By adding the appropriate fire retardant elements into UV-curable matrices, i.e., boron, phosphorus, and silicone, the resulting coating can provide the underlying material with good flame retardant properties. Cationic UV-curable materials, such as epoxy resins in particular, have the advantages of efficient adhesion, low shrinkage, and absence of oxygen inhibition.<sup>18</sup> Cycloaliphatic epoxy resins are widely used as encapsulants in microelectronic industry for high photopolymerization activity.<sup>19, 20</sup> Although it has a number of benefits during application, the UV curable cycloaliphatic epoxide does not exhibit sufficient flame retardancy and is easily burned. The most commonly used cycloaliphatic epoxy resin 3,4-epoxycyclohexylmethyl-3,4-epoxycyclohexane carboxylate has a low limiting-oxygen index of ~18 and a low melting viscosity, which can cause dripping in flame.<sup>19</sup>

9, 10-Dihydro-9-oxa-10-phosphaphenanthrene-10-oxide (DOPO) and its derivatives have received considerable attention as novel phosphorus-containing flame retardants in epoxy resins.<sup>21-25</sup> DOPO reacts with electron-deficient compounds, and some excellent flame retardants can be obtained when

DOPO is introduced into the chemical structure containing nitrogen. However, such products usually have high melting points and are difficult to dissolve into the cycloaliphatic epoxides. Silicone compounds are among the best modifiers for epoxy resins because of their superior thermal and thermo-oxidative stabilities.<sup>26</sup> Moreover, phosphorus and silicon elements have been developed because of their excellent carbonization and flame retardancy.<sup>27</sup> Moreover, several silicone compounds exhibit good solubility in epoxy resins. However, only few works have investigated the synergistic flame retardancy effect of the compounds containing phosphorus, nitrogen, and silicon on the UV-curable epoxy resins.

To develop efficient flame retardants based on synergistic combinations of silicon and other elements and solve the incompatibility of flame retardants with epoxy resins, two novel reactive-type phosphorus-nitrogen-silicon flame retardants containing were obtained via a simple and efficient synthesis. Flame-retardant epoxy composites (FR-Ep) with different contents of PNSi were prepared from ERL4221 and cross-linked through UV-radiation. The effects of PNSi on the flame-retardant properties and thermal stabilities of FR-Ep were investigated by limiting oxygen index (LOI) tests, vertical burning tests (UL-94), and thermogravimetric analysis (TGA).

## Experimental details

### Materials and characterization

1,1,1,3,5,5,5-heptamethyltrisiloxane (HMS, Jiangxi Duolin CO., Ltd, China) and amino silicone oil (SiONH<sub>2</sub>, Shin-Etsu Chemical Industrial CO., Ltd, China) was reagent quality and used without further purification. 9, 10-dihydro-9-oxa-10-phosphaphenanthrene-10-oxide (DOPO) was purchased from Huizhou Sunstar Technology CO., Ltd (China). The commercial epoxy compounds used in this work is 3, 4-epoxycyclohexylmethyl-3, 4-epoxycyclohexane carboxylate (ERL4221, epoxy value: 0.78 mol/100g) which was purchased from Jiangsu Tetrachem CO., Ltd (China). Lamoreaux's catalyst and the cationic photoinitiator cyclopentadienyl iron complex of carbazole (In-Fe) were self-prepared with the reported method.<sup>19, 28</sup> Other reagents and solvents were commercially available and reagent quality. The structures of SiONH<sub>2</sub>, HMS, ERL4221 and In-Fe employed in this study were summarized in Fig. 1.

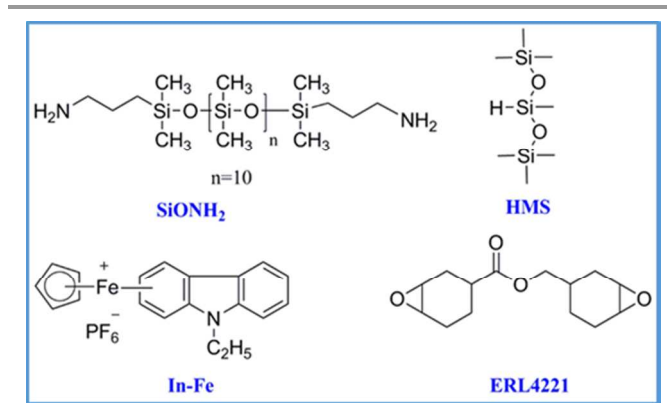


Fig. 1. Structures of SiONH<sub>2</sub>, HMS, ERL4221 and In-Fe.

The FT-IR spectra (scanned between 400 and 4000 cm<sup>-1</sup>) were obtained on a Nicolet 50XC spectrometer (Nicolet, USA). The <sup>1</sup>H-NMR and <sup>31</sup>P-NMR spectra were recorded on an AV400 unity spectrometer (Bruker, USA) operated at 400 MHz with CDCl<sub>3</sub> or DMSO-*d*<sub>6</sub> as solvent and tetramethylsilane as an internal standard. Light intensity was recorded by a UV light radiometer (Photoelectric Instrument Factory, Beijing Normal University, China). The thermogravimetric analysis (TGA) was performed on STA-449C simultaneous thermal analyzer (Netzsch, Germany) with a heating rate of 10°C/min under high purity nitrogen condition and the mass of each sample was approximately 3~10 mg. The limiting oxygen index (LOI) tests were carried out on a JF-3 type instrument (Jiangning, China), according to GB/T 2406-1993. The specimens used for the test were of dimensions 100 mm×6.5 mm×3 mm. The percentage of O<sub>2</sub> in the O<sub>2</sub>/N<sub>2</sub> mixture was taken as the LOI which was just sufficient to sustain the combustion of plastics. The UL-94 vertical test was carried out on CZF-3 instrument (Jiangning Analysis Instrument Co. China) according to the UL-94 standard. The specimens used for the test were of dimensions 130 mm×13 mm×3 mm. The gases evolved during TGA tests were analyzed by coupling TGA with FTIR spectroscopy. Char residues after LOI tests were carried out on Hitachi S-4700 (Hitachi, Japan) scanning electron microscope (SEM). The hardness of the materials was measured at room temperature using a XY-1 Durometer (Shore D, Shanghai, China). All of the values were determined using averages of three repetitions for each material composition to obtain a reliable average value.

### Synthesis of 3-aminopropyltrisiloxane (APTS)

HMS (0.2 mol, 44.50 g), Lamoreaux's catalyst (6.60 μmol Pt) and 100ml toluene were placed into a 250 mL three-necked flask with a mechanical stirrer, reflux condenser, and dropping funnel under a nitrogen atmosphere. The reaction mixture was stirred at 50 °C for 0.5 h. Then the oil temperature was raised to 100 °C, the allylamine (0.24 mol, 13.71 g) was added dropwise for about 5 h and further reacted for about 4 h. The product was distilled under a reduced pressure of 25 mm Hg at about 120 °C, and the colorless liquid mixture APTS were obtained (28.7 g, yield: 51.4%). FT-IR (KBr) ν<sub>max</sub> (cm<sup>-1</sup>): 3420(-NH<sub>2</sub>), 2951~2849 (CH<sub>3</sub> and CH<sub>2</sub>), 1257 (Si-CH<sub>3</sub>), 1060 (Si-O-Si); <sup>1</sup>H

NMR ( $\text{CDCl}_3$ , 400MHz)  $\delta_{\text{ppm}}$ : 0.01 (3H, -Si-CH<sub>3</sub>), 0.09 (18H, -O-Si(CH<sub>3</sub>)<sub>3</sub>), 0.43-0.47, 2.52-2.57 (2H, H<sub>3</sub>+H<sub>3'</sub>), 0.95~0.97, 1.41~1.49 (2H, H<sub>2</sub>+H<sub>2'</sub>), 2.64~2.68, 2.84~2.88 (2H, H<sub>1</sub>+H<sub>1'</sub>), 1.14 (2H, NH<sub>2</sub>).

### Synthesis of PSAP

APTS (0.12 mol, 33.55 g), 4-hydroxybenzaldehyde (0.10 mol, 12.21 g) and 100 mL dichloromethane were introduced into a round-bottom 250 mL glass flask equipped with a nitrogen inlet, a condenser, and a magnetic stirrer. The reaction mixture was stirred at room temperature for about 4 h until complete conversion of 4-hydroxybenzaldehyde and APTS, as confirmed by IR and TLC. DOPO (0.10 mol, 21.62 g) was added into the system, and then further reacted at room temperature for about 9 h. After complete conversion of DOPO tested via TLC, the solvent was removed using a rotary evaporator. The residual solid was recrystallized from ethyl acetate to give white powder named PSAP. The obtained PSAP is a mixture of two isomers (49.8 g, yield: 83.2%). FT-IR (KBr)  $\nu_{\text{max}}$  (cm<sup>-1</sup>): 3217 (-OH), 2951~2849 (CH<sub>3</sub> and CH<sub>2</sub>), 1612, 1595, 1514, 1476 (Ar ring skeleton stretch), 1206 (P=O), 1257 (Si-CH<sub>3</sub>), 1047 (Si-O-Si), 921 (P-O-C); <sup>1</sup>H NMR (DMSO-*d*<sub>6</sub>, 400MHz):  $\delta_{\text{ppm}}$  = -0.13~0.08 (21H, -Si-CH<sub>3</sub>), 0.18~0.25 (m, 2H), 1.24 (m, 2H), 2.25~2.28 (m, 2H), 2.39 (s, 1H), 4.20~4.23 (q, 1H), 6.56 (d, 2H), 6.96 (d, 2H), 7.19~7.27 (q, 2H), 7.39~7.49 (m, 2H), 7.64~7.75 (m, 2H), 8.06~8.17 (m, 2H), 9.30 (1H, -OH); <sup>31</sup>P NMR (DMSO-*d*<sub>6</sub>, 161MHz):  $\delta_{\text{ppm}}$  = 32.32; MS: *m/z* = 601 (M+1<sup>+</sup>).

### Synthesis of DPP-Si

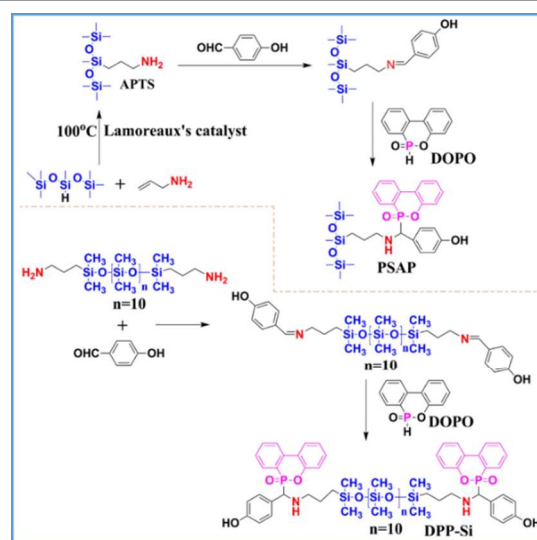
The preparation of DPP-Si was same to the means of PASP, except that SiONH<sub>2</sub> was used instead of APTS. The obtained DPP-Si was a yellow solid (24.8 g, yield: 79.5%). FT-IR (KBr)  $\nu_{\text{max}}$  (cm<sup>-1</sup>): 3305 (-OH); 2954~2846 (CH<sub>3</sub> and CH<sub>2</sub>); 1606, 1523, 1452 (Ar ring); 1187 (P=O); 1267 (Si-CH<sub>3</sub>), 1040~1092 (Si-O-Si); 921 (P-O-C); <sup>1</sup>H NMR ( $\text{CDCl}_3$ , 400MHz):  $\delta_{\text{ppm}}$  = -0.14~0.21 (-Si-CH<sub>3</sub>), 0.25~0.35 (m, Si-CH<sub>2</sub>), 1.25~1.39 (m, Si-CH<sub>2</sub>-CH<sub>2</sub>-), 2.21~2.58 (m, -NH-+-NH-CH<sub>2</sub>-), 4.01~4.22 (d, -P-CH-), 6.57~8.06 (m, Ar-H), 9.83 (s, -OH); <sup>31</sup>P NMR ( $\text{CDCl}_3$ , 161MHz)  $\delta_{\text{ppm}}$  = 11.56.

### Sample preparation

The epoxy monomer ERL4221 was oven-dried at 120 °C for 3 h to remove the moisture before it was processed. ERL4221 and the flame-retardant PNSi were mixed thoroughly at 100 °C. After the mixtures had cooled to 40 °C, 4.0 wt % cyclopentadienyliron complex of carbazole (In-Fe) used as photoinitiator was added and mixed. The mixtures were then exposed to a high pressure Hg lamp ( $\lambda_{\text{max}}$  = 365 nm, *I* = 1 mW·cm<sup>-2</sup>) for 20 min and heated in an oven for thermal post-curing at 120 °C for 30 min.

## Results and discussion

### Synthesis and characterization.



Scheme 1. The synthesis routes of PSAP and DPP-Si.

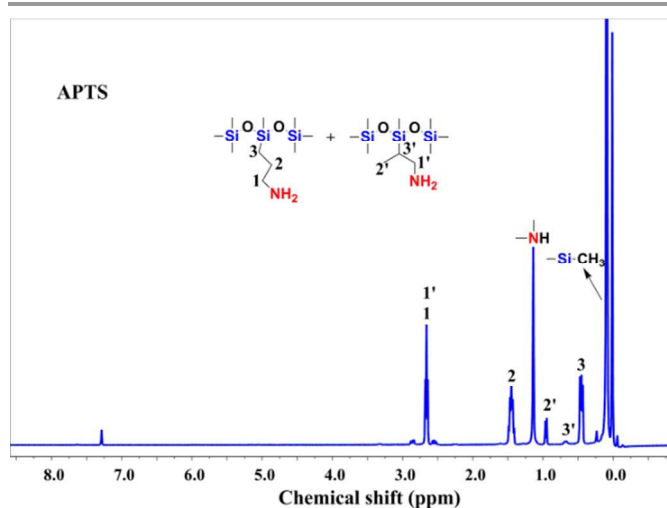


Fig. 2. <sup>1</sup>H NMR spectra of APTS.

In this paper, APTS was obtained via hydrosilylation reaction between Si-H and 3-aminopropene and catalyzed by Lamoreaux's catalyst.<sup>29, 30</sup> The intermediates containing C=N group were then obtained from the reaction of 4-hydroxybenzaldehyde with amino siloxanes. Primary amine undergoes nucleophilic addition reaction with aldehyde, and imine is then obtained after dehydration. The target products were obtained from the addition reaction of DOPO and the intermediates containing C=N group. The P-H bond in DOPO is very active because it can easily react with C=N at room temperature. Therefore, the whole reaction was carried out in a short period. The synthesis routes of PSAP and DPP-Si are presented in Scheme 1.

From the <sup>1</sup>H NMR spectrum of APTS (Fig. 2), the two isomers were simultaneously obtained from the hydrosilylation reaction between Si-H and 3-aminopropene and catalyzed by Lamoreaux's catalyst. The  $\gamma$ -aminopropyl trisiloxane is the main product of the vinyl carbon activity and the stereoscopic space effect. These two isomers were not separated in this study

because they have similar boiling points and polarities. Therefore, the flame retardant also exists in a mixture of PSAP and PSAP, as confirmed by the  $^1\text{H}$  NMR spectra of PSAP (Fig. 3).

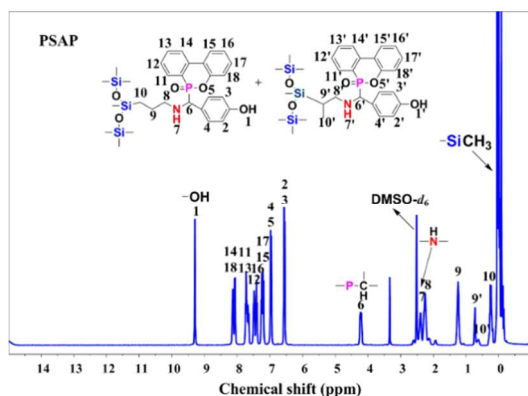


Fig. 3.  $^1\text{H}$  NMR spectra of PSAP.

The chemical structures of DPP-Si and PSAP were characterized via FTIR,  $^1\text{H}$  NMR, and  $^{31}\text{P}$  NMR. Fig. 4 shows the FTIR spectra of DPP-Si and PSAP. The absorptions at 1612, 1595, and 1476  $\text{cm}^{-1}$  indicate that the PSAP contains aromatic rings. In addition, the peak at 1206  $\text{cm}^{-1}$  is assigned to P=O stretching vibration. The peak at 1057  $\text{cm}^{-1}$  is assigned to the Si-O-Si stretching vibration. The peak at 921  $\text{cm}^{-1}$  is attributed to the P-O-C stretching vibration.

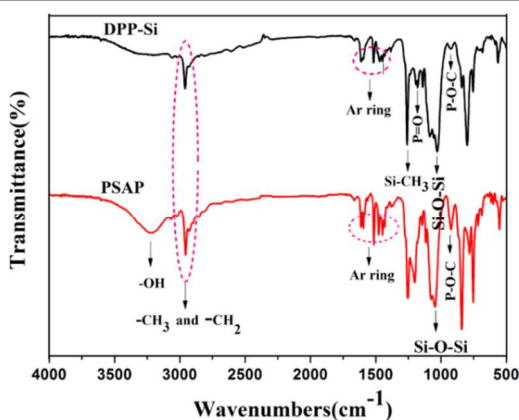


Fig. 4. FT-IR spectra of DPP-Si and PSAP.

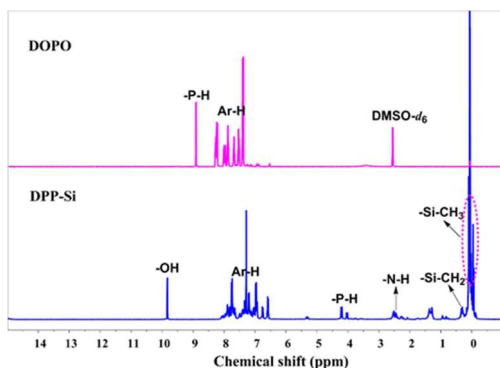


Fig. 5.  $^1\text{H}$  NMR spectra of DOPO and DPP-Si.

The  $^1\text{H}$  NMR spectra of DOPO and DPP-Si are shown in Fig. 5. The peaks at 6.5 ppm to 8.2 ppm are attributed to the protons in the benzene ring. The peak occurred at 2.39 ppm is assigned to the proton in -NH-. The protons in the -(SiCH<sub>2</sub>CH<sub>2</sub>CH<sub>2</sub>N)-moiety are at 0.43 to 0.47 (-CH<sub>2</sub>-Si), 1.24 (C-CH<sub>2</sub>-C) and 2.28 (CH<sub>2</sub>N). The  $^{31}\text{P}$  NMR spectra of DOPO and PSAP are displayed in Fig. 6. Based on the  $^{31}\text{P}$  NMR spectrum of DPP-Si, new chemical shifts was observed at about 11.56 ppm, and no peaks corresponding to DOPO. In the  $^{31}\text{P}$  NMR spectrum of PSAP, a new peak was observed at about 32.3 ppm. All these absorptions indicate the formation of new flame retardants.

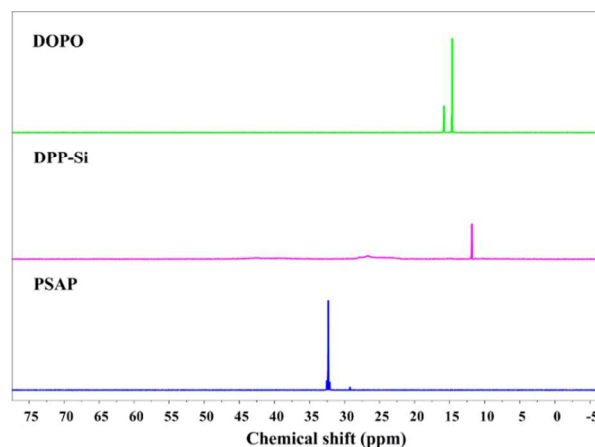


Fig. 6.  $^{31}\text{P}$  NMR spectra of DOPO, DPP-Si and PSAP.

#### Compatibility of DOPO, PSAP and DPP-Si with ERL4221

The solubility parameters of DOPO, PSAP and DPP-Si in ERL4221 were measured. It can be observed obviously that the solubility of PSAP or DPP-Si in ERL4221 far outweigh that of DOPO shown in Table 1. This could be attributed to the siloxanes introduced into the flame retardants which can improve the integral solubility of flame retardants in ERL4221. Moreover, the better solubility is possibly owing to the hydroxyl group of DPP-Si and PASP.<sup>29</sup>

Table 1. The solubility of DOPO, PSAP and DPP-Si in ERL4221.

Samples	Solubility in ERL4221 (g/100g)		
	50 °C	75 °C	100 °C
DOPO	0.22	0.34	0.53
PSAP	7.52	11.38	15.87
DPP-Si	7.26	10.97	15.59

#### The thermal stabilities of DPP-Si and PSAP

The thermal stabilities of DPP-Si and PSAP were measured by TGA in nitrogen. The TGA and DTG curves are shown in Fig. 7 and the thermal decomposition data are listed in Table 2. As shown in Figs. 7a and 7b, both DPP-Si and PSAP show good thermal stability under 200 °C. The temperature at which the weight loss is about 10 wt % DPP-Si is at 267 °C, which is higher than that of PSAP.

Table 2. The thermal decomposition data of the flame retardants.

Samples	$T_{0.1}^{\alpha}$ °C	$T_{max}^{\beta}$ °C	$T_{max}^2$ °C	Char (wt%, 800 °C)
DPP-Si	267	330	/	20.7
PSAP	217	222	468	10.3

$\alpha$ :  $T_{0.1}$  is the temperature at which the weight losses is 10 wt %;  $\beta$ :  $T_{max}$  is the temperature at the maximum weight loss rate.

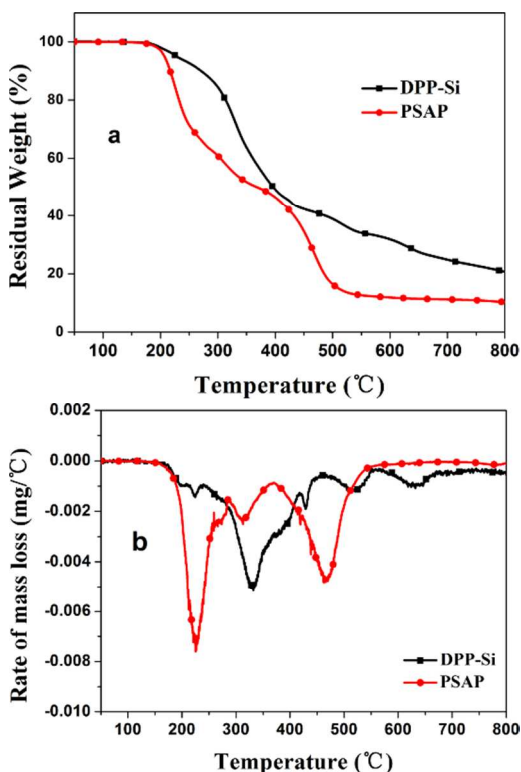


Fig. 7. TGA (a) and DTG (b) curves of DPP-Si and PSAP in nitrogen.

### Hardness (Shore D) of FR-Ep bars

Hardness is one of the most important parameters to characterize the mechanical properties of the polymer. Hardness behavior of each FR-Ep bars with an increasing mass fraction of DPP-Si or PSAP is shown in Fig. 8. It can be observed that the hardness value of each FR-Ep was higher than Ep-0 and Ep-DOPO, and the hardness of the FR-Ep bar was gradually increased with an increasing mass fraction of DPP-Si or PSAP. This could be attributed to the gradual increase of content of siloxane-containing flame retardants, leading to the gradual increase of the crosslinking points in the polymer.<sup>29-32</sup>

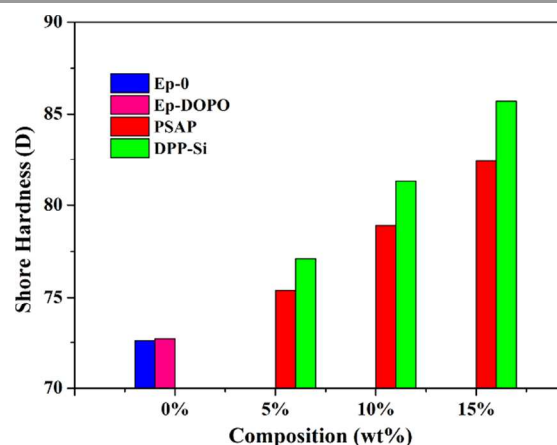


Fig. 8. The variation of FR-Ep composite hardness as a function of PSAP or DPP-Si content. (Ep-DOPO containing 2 wt% DOPO, but can't be completely soluble in ERL4221)

### Flame-retardant properties of FR-Ep.

The effect of DPP-Si and PSAP on the flame retardancy of cured cycloaliphatic epoxy resins (FR-Ep) was evaluated based on LOI and on result of UL-94 test. The results, as well as the formulations of FR-Ep composites are shown in Table 3. Pure epoxy resin (Ep-0) is highly combustible at an LOI value of 20.5% and is not classified in the UL-94 rating. The LOI values increase with the addition of DPP-Si and PSAP into the FR-Ep composites. When FR-Ep-3 composites were added with 15 wt % DPP-Si, the LOI value of FR-Ep-3 reaches 27.2% and the flame retardancy passed the V-1 rating. The effect of PSAP on the flame retardancy of FR-Ep is similar to the effect of DPP-Si. When FR-Ep composites were added with 15 wt % PSAP, the LOI value of FR-Ep-6 reaches 27.6% and the flame retardancy also passed the V-1 rating.

Table 3. Compositions and Flame Retardancy of the cured Cycloaliphatic Epoxy Resins.

Flame retarded epoxy resin	DPP-Si (wt%)	PSAP (wt%)	Element content			LOI (%)	UL-94*
			P(wt%)	Si(wt%)	N(wt%)		
Ep-0	0	0	0	0	0	20.5	NR
FR-Ep-1	5	0	0.19	1.03	0.09	22.8	NR
FR-Ep-2	10	0	0.38	2.07	0.17	26.6	V-1
FR-Ep-3	15	0	0.57	3.10	0.26	27.2	V-1
FR-Ep-4	0	5	0.26	0.70	0.12	23.4	NR
FR-Ep-5	0	10	0.52	1.40	0.24	26.8	V-1
FR-Ep-6	0	15	0.77	2.11	0.35	27.6	V-1

\*NR, No rating; V-1, Burning stops within 60s after two applications of ten seconds each of a flame to a test bar. No flaming drips are allowed; V-2, Burning stops within 60s after two applications of ten seconds each of a flame to a test bar. Flaming drips are allowed.

The LOI values of FR-Ep increased from 20.5% to around 27.6% when the phosphorus content was increased from 0 wt % (Ep-0) to about 0.77 wt % (FR-Ep-6). Thus, the presence of phosphorus increases the LOI values even at low contents, and

the silicon-nitrogen-phosphorus synergistic effect might have contributed to the excellent flame retardancy of this system.

### Thermal stability of FR-Ep.

The thermal decomposition behavior of the cured FR-Ep systems was investigated via TGA of nitrogen. The TGA thermograms and the differential weight loss (DTG) curves of FR-Ep-1, FR-Ep-2 and FR-Ep-3 in a nitrogen atmosphere are shown in Figs. 9a and b. The TGA and DTG curves of FR-Ep-4, FR-Ep-5 and FR-Ep-6 are shown in Figs 9c and d. For comparison, the TGA and the DTG curves of Ep-0 were likewise obtained. The specific degradation temperatures and the final char yield at 800 °C are summarized in Table 4.

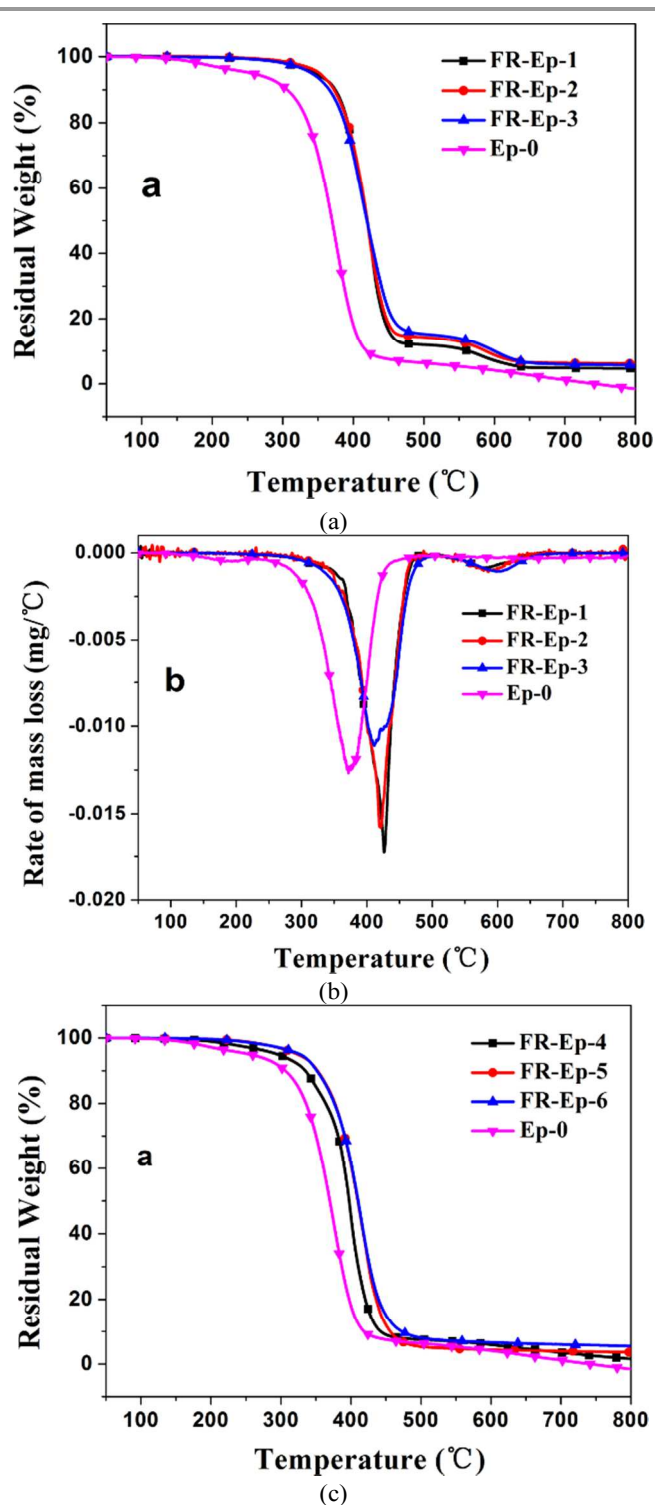
The  $T_{0.1}$  and  $T_{max}$  of Ep-0 are about 306 °C and 375 °C. the  $T_{0.1}$  and  $T_{max}$  of Ep-DOPO are about 311 °C and 379 °C. However, the  $T_{0.1}$  and  $T_{max}$  of FR-Ep-1 in which 5 wt % DPP-Si was added, are about 374 °C and 426 °C. Similar results were observed in FR-Ep-4. When the content of DPP-Si and FASP was increased, the change in thermal stability of FR-Ep is little. The addition of DPP-Si and PASP in FR-Ep results in the increase of  $T_{0.1}$  and  $T_{max}$  of the flame-retarded FR-Ep composites, which is possibly owing to the fact that DPP-Si and PASP own active hydroxyl group which can react with the epoxy group (Fig. 10). That makes the cross density of cured FR-Ep higher than that of pure Ep-0 and Ep-DOPO. The better thermal stability of FR-Ep also indicates that the addition of DPP-Si and PASP in FR-Ep did not affect the curing of FR-Ep, even though different the adding-type flame retarded composites were different.

The resulting char residue of pure Ep-0 and Ep-DOPO at 800 °C is 1.5 wt % and 1.8%. The char residues at 800 °C of the FR-Ep composites are improved with the addition of DPP-Si and PSAP, which can protect the materials from the heat stress.

**Table 4.** The thermal decomposition data of FR-Ep.

Samples	DPP-Si (wt%)	PSAP (wt%)	$T_{0.1}$ °C	$T_{max}$ °C	Char (800°C) wt%
EP-0	0	0	306	375	1.5
Ep-DOPO	0	0	311	379	1.8
FR-Ep-1	5	0	374	426	4.6
FR-Ep-2	10	0	373	421	6.1
FR-Ep-3	15	0	367	412	5.7
FR-Ep-4	0	5	335	399	1.6
FR-Ep-5	0	10	352	419	3.6
FR-Ep-6	0	15	351	415	5.5

(Ep-DOPO containing 2wt% DOPO, but can't be completely soluble)



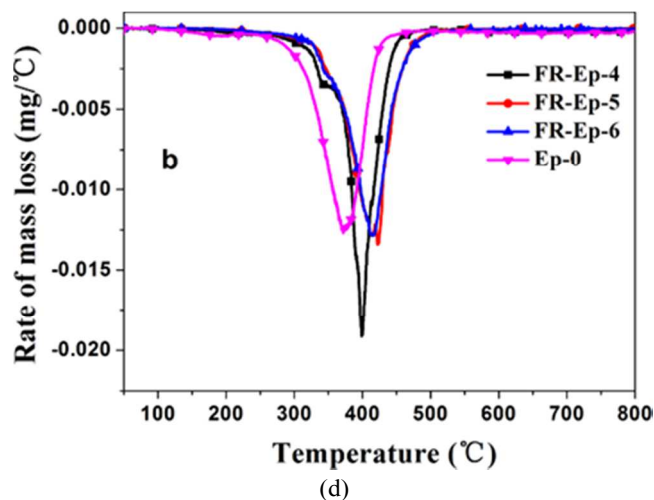


Fig. 9. TGA and DTG curves of FR-Ep epoxy systems.

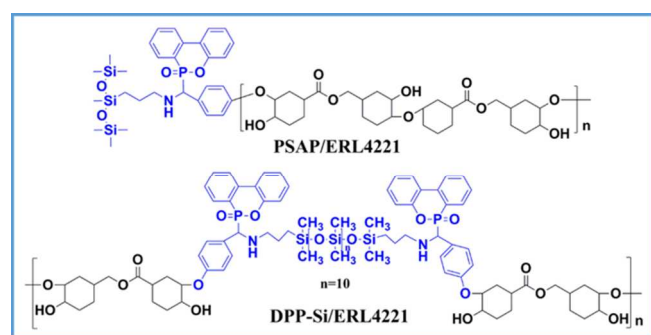


Fig. 10. Structure of FR-Ep containing DPP-Si and PSAP.

Based on the TG-IR curves of the flame-retardant epoxy composites (FR-Ep), several representative temperatures (such as 300 °C, 360 °C, 380 °C, 420 °C, 460 °C, 480 °C, 530 °C, and 580 °C) were selected to investigate the volatile components released during the thermal degradation process. Fig. 11 shows the TG-IR spectra of the volatilized products at typical temperatures during the thermal degradation of the FR-Ep. Taking FR-Ep-6 at 300 °C, the absorption peaks at 2362  $\text{cm}^{-1}$  to 2321  $\text{cm}^{-1}$ , which correspond to  $\text{CO}_2$ , are clearly observed in the spectrum and is caused by the break of the C–O–C structure from the matrix of the epoxy.<sup>33, 34</sup> The peaks (670, 2362, and 2321  $\text{cm}^{-1}$ ) become stronger with increasing temperature, which suggests that a large amount of  $\text{CO}_2$  was released.<sup>35</sup> When the temperature was increased, intensive absorption peaks were also found at 3500  $\text{cm}^{-1}$  to 3900  $\text{cm}^{-1}$ , which indicates that the volatilized products contain  $\text{H}_2\text{O}$ .<sup>36</sup> At 360 °C, the appearance of the new peak (1259  $\text{cm}^{-1}$  is assigned to the P=O bond) and the other peaks (902  $\text{cm}^{-1}$  to 848  $\text{cm}^{-1}$  is attributed to the P–O–C bond) indicates the initial breakdown of the flame retardants.<sup>37</sup> The peaks (3044, 1600 to 1300, and 1850 to 1611  $\text{cm}^{-1}$ ) become gradually stronger with increasing temperature, which suggests that the volatile products contain aromatic rings and carbonyl-containing compounds.<sup>37, 38</sup> When the temperature was further increased to 420 °C, new peaks, representing the aliphatic components (2950 and 2875  $\text{cm}^{-1}$ ), appear which demonstrate the decomposition of the

aminopropyl.<sup>33, 39</sup> These complex reactions lead to the formation of the compact Si–O–Si char layer; thus, the appearances of these peaks also reflect the process of the char formation.

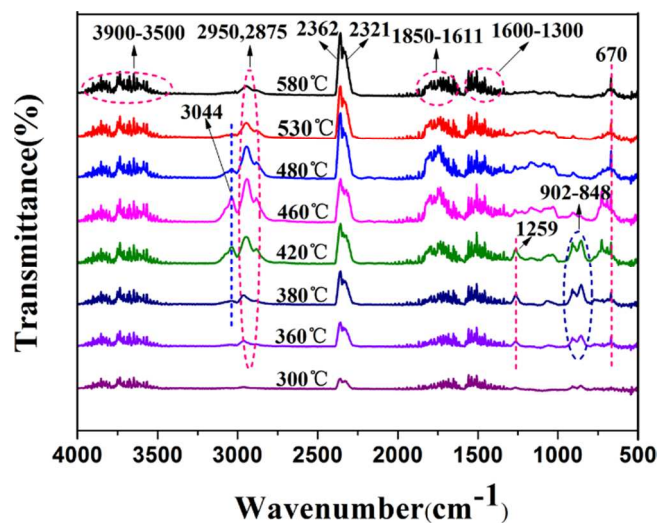


Fig. 11. TG-IR spectra of volatilized products at typical temperatures during the thermal degradation of the FR-Ep-6 under a  $\text{N}_2$  atmosphere.

### Morphology of the residues' char

The morphology of the char residue after the LOI tests was further investigated via SEM test, as shown in Fig. 12. The char surfaces of FR-Ep-3, as illustrated on Figs. 12a and 11b, are compact, tight, and smooth. Such characteristics can effectively prevent the underlying polymer from heat and can also make the material less susceptible to cracks.<sup>34, 40</sup> The inner surface of the char of FR-Ep-3, illustrated on Fig. 11b shows some little holes from gases produced when burnt.<sup>33</sup> The formed gas effectively prevents the tightening of the char, and no hole on the outer surface of the char was observed. Those properties are in agreement with the improvement in flame retardancy.

Relative to FR-Ep-3, the char surfaces of FR-Ep-6 illustrated on Figs. 12a and b are a little loose, and more gas holes in the inner surface of the char were observed. The possible reason is that the nitrogen content of FR-Ep-6 is higher than that of FR-Ep-3, and the silicon content of FR-Ep-6 is lower than that of FR-Ep-3. Hence, we can infer that the tight char surface is mainly caused by the compound containing silicon. To further demonstrate the viewpoint mentioned here, the FTIR spectra of the char were investigated.

Fig. 13 shows the FTIR spectra of the char from FR-Ep-3 and FR-Ep-6. The FTIR spectrum of the char of FR-Ep-3 is almost same with that of FR-Ep-6. The absorbing peak between 1100 and 1000  $\text{cm}^{-1}$ , is strong and assigned to the stretching vibration bond of Si–O–Si.<sup>41, 42</sup> The results indicate that the char residues mainly consist of Si–O–Si structures, which function as a protective barrier that separates heat and cuts off oxygen.

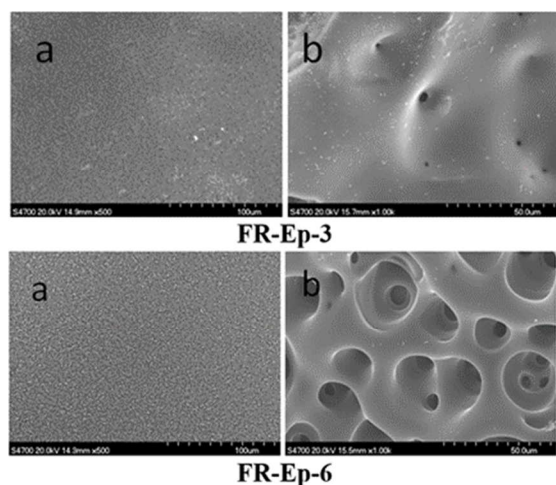


Fig. 12. SEM morphology of the char residues of FR-Ep: outer surface (a) and inner surface (b).

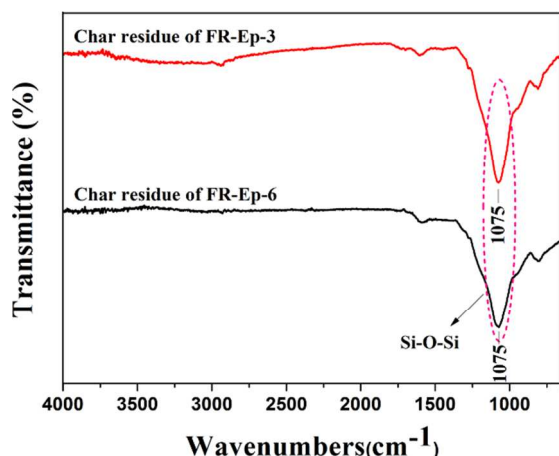
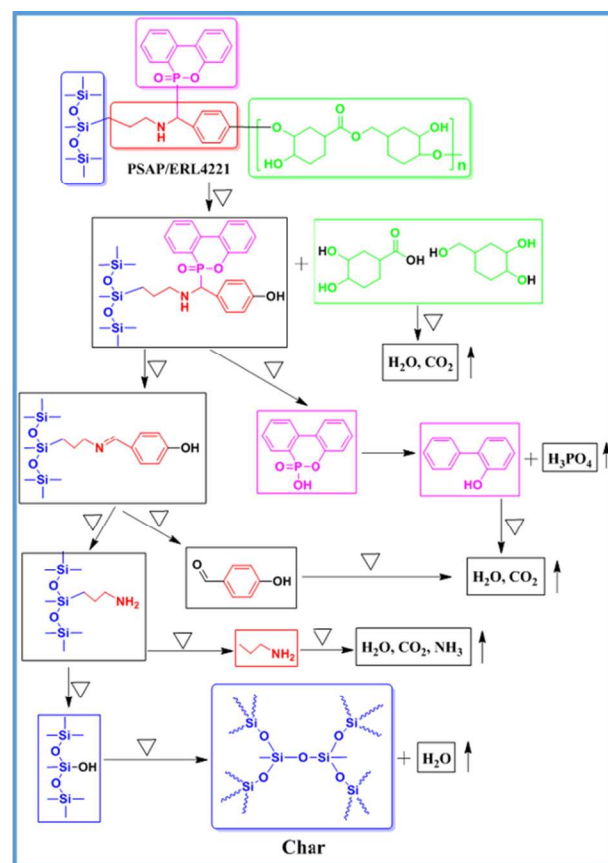


Fig.13. IR spectra of the char residue for FR-Ep-3 and FR-Ep-6 after LOI test.

According to the TG-IR, SEM and FT-IR tests results combined with the reports in the literature,<sup>36, 45-51</sup> taking FR-Ep-6 for example, the possible thermal degradation mechanism on charring for FR-Ep-6 during the combustion is proposed in Scheme 2. It can be concluded as follows: in the initial stage, when the modified FR-Ep is heated, the C–O–C groups from ERL4221 and formed between the hydroxyl of PSAP and ERL4221 were broken, and released gases such as CO<sub>2</sub> and H<sub>2</sub>O during the combustion process. In addition, with increasing the temperature, the C–N–C structures in PSAP were decomposed accompanied by forming some amine groups and formyl groups simultaneously. Then, along with the release of NH<sub>3</sub>, H<sub>2</sub>O, and CO<sub>2</sub> the aminopropyl decomposes completely to produce a great amount of siloxanes containing active hydroxyl which promoted the formation of tight, smooth, compact, and stable char layer through condensation reaction. Finally, the excellent flame retardant performance of FR-Ep was achieved.



Scheme 2. Possible thermal degradation mechanism on charring for FR-Ep-6

## Conclusion

In this paper, two novel flame retardants, DPP-Si and PSAP, were prepared via a simple way. This result proves that DPP-Si and PSAP have excellent flame retardancy, and good compatibility with cycloaliphatic epoxy ERL4221. At 15 wt % loading of DPP-Si or PSAP, the LOI value of FR-Ep composites increases from 20.5% to 27.6%. The addition of DPP-Si and PSAP in FR-Ep results in an increase in the thermal stabilities of the flame-retarded FR-Ep composites. From the analysis of SEM and FTIR spectra, a dense and compact graphitized layer composed of silicon is formed, which prevents the materials from burning.

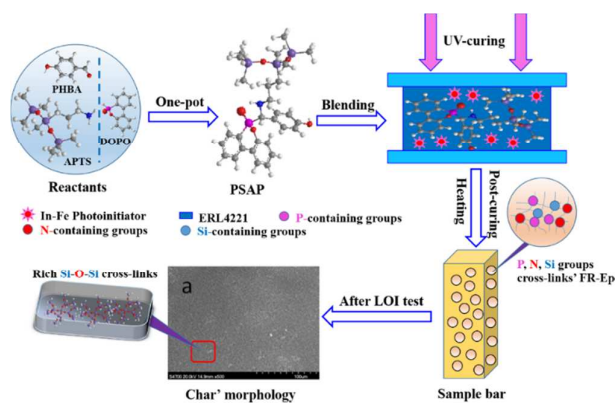
## Acknowledgements

The authors wish to thank for financial supports of national natural science foundation of China (Project Grant No. 21176016).

## Notes and references

<sup>1</sup>State Key Laboratory of Chemical Resource Engineering, College of Science, Beijing University of Chemical Technology, Beijing 100029, PR China, Tel.: 0086-010-64445350, E-mail: wangtwj2000@163.com

- <sup>2</sup>Department of Organic Chemistry, College of Science, Beijing University of Chemical Technology, Beijing 100029, PR China
- <sup>3</sup>College of Materials Science and Engineering, Beijing University of Chemical Technology, Beijing, 100029, PR China
- †Electronic Supplementary Information (ESI) available: [details of any supplementary information available should be included here]. See DOI: 10.1039/b000000x/
- 1 X. Wang, Y.T. Pan, J.T. Wan and D.Y. Wang, *RSC Adv.*, 2014, **4**, 46164-46169.
  - 2 C. Ruan, K. Ai, X. Li and L. Lu, *Angew. Chem., Int. Ed.*, 2014, **53**, 5556-5560.
  - 3 W. Ding, J. Li and K. Tao, *RSC Adv.*, 2014, **4**, 34161-34167.
  - 4 D. Patra, P. Vangal, A. A. Cain, C. Cho, O. Regev and J. C. Grunlan, *ACS Appl. Mater. Interfaces*, 2014, **6**, 16903-16908.
  - 5 S. Chang, R. P. Slopek, B. Condon and J. C. Grunlan, *Ind. Eng. Chem. Res.*, 2014, **53**, 3805-3812.
  - 6 K. Apaydin, A. Laachachi, T. Fouquet, M. Jimenez, S. Bourbigot and D. Ruch, *RSC Adv.*, 2014, **4**, 43326-43334.
  - 7 Y.C. Li, Y. S. Kim, J. Shields and R. Davis, *J. Mater. Chem. A*, 2013, **1**, 12987-12997.
  - 8 J.P. Cao, X. Zhao, J. Zhao, J.W. Zha, G.-H. Hu and Z.M. Dang, *ACS Appl. Mater. Interfaces*, 2013, **5**, 6915-6924.
  - 9 J. Alongi, C. Colleoni, G. Rosace and G. Malucelli, *Polym. Degrad. Stab.*, 2013, **98**, 579-589.
  - 10 S. Ravichandran, S. Nagarajan, B. C. Ku, B. Coughlin, T. Emrick, J. Kumar and R. Nagarajan, *Green Chem.*, 2012, **14**, 819-824.
  - 11 M. Moreno, G. Lligadas, J. C. Ronda, M. Galia and V. Caldiz, *J. Polym. Sci., Part A: Polym. Chem.*, 2012, **50**, 4368.
  - 12 B.Y. Ryu and T. Emrick, *Macromolecules (Washington, DC, U. S.)*, 2011, **44**, 5693-5700.
  - 13 J.S. Lin, Y. Liu, D.Y. Wang, Q. Qin and Y.Z. Wang, *Ind. Eng. Chem. Res.*, 2011, **50**, 9998-10005.
  - 14 Y. Chen, J. Zhan, P. Zhang, S. Nie, H. Lu, L. Song and Y. Hu, *Ind. Eng. Chem. Res.*, 2010, **49**, 8200-8208.
  - 15 Z. Guo, X. Zhang, X. Yan, J. Guo, D. Jiang, Q. He, H. Wei, H. Gu, Z. Liu, H. A. Colorado, X. Zhang and S. Wei, *J. Mater. Chem. C*, 2014, Ahead of Print.
  - 16 X. Wang, J. Zhan, W. Xing, X. Wang, L. Song, X. Qian, B. Yu and Y. Hu, *Ind. Eng. Chem. Res.*, 2013, **52**, 5548-5555.
  - 17 X. Qian, H. Pan, Y. X. Wei, L. Song, R. K. K. Yuen and Y. Hu, *Ind. Eng. Chem. Res.*, 2012, **51**, 85-94.
  - 18 T. Wang, H. Ye, X. Zhang and J. Cheng, *Ind. Eng. Chem. Res.*, 2012, **51**, 15832-15838.
  - 19 Y.J. Li, X.Y. Gu, J. Zhao, P. Jiang, J. Sun and T. Wang, *J. Appl. Polym. Sci.*, 2014, **131**, 40011/40011-40011/40017.
  - 20 W. Liu, Z. Wang, Z. Chen, J. Li and L. Zhao, *Polym. Adv. Technol.*, 2012, **23**, 367-374.
  - 21 Z. Zhang, L. Yuan, G. Liang, A. Gu, Z. Qiang, C. Yang and X. Chen, *J. Mater. Chem. A*, 2014, **2**, 4975-4988.
  - 22 L. Yu, L. Chen, L.P. Dong, L.J. Li and Y.Z. Wang, *RSC Adv.*, 2014, **4**, 17812-17821.
  - 23 X. Chen, J. Ye, L. Yuan, G. Liang and A. Gu, *J. Mater. Chem. A*, 2014, **2**, 7491-7501.
  - 24 X. Qian, L. Song, S. Jiang, G. Tang, W. Xing, B. Wang, Y. Hu and R. K. K. Yuen, *Ind. Eng. Chem. Res.*, 2013, **52**, 7307-7315.
  - 25 I.D. Carja, D. Serbezeanu, T. Vlad-Bubulac, C. Hamciuc, A. Coroaba, G. Lisa, C. G. Lopez, M. F. Soriano, V. F. Perez and M. D. Romero Sanchez, *J. Mater. Chem. A*, 2014, **2**, 16230-16241.
  - 26 H. Singh and A. K. Jain, *J. Appl. Polym. Sci.*, 2009, **111**, 1115-1143.
  - 27 F. Liao, L. Zhou, Y. Ju, Y. Yang and X. Wang, *Ind. Eng. Chem. Res.*, 2014, **53**, 10015-10023.
  - 28 D.W. Chung and T. G. Kim, *J. Ind. Eng. Chem. (Seoul, Repub. Korea)*, 2007, **13**, 571-577.
  - 29 J.Y. Bae, Y. Kim, H.Y. Kim, Y.W. Lim and B.S. Bae, *RSC Adv.*, 2013, **3**, 8871-8877.
  - 30 K. Igawa, D. Yoshihiro, N. Ichikawa, N. Kokan and K. Tomooka, *Angew. Chem., Int. Ed.*, 2012, **51**, 12745-12748.
  - 31 W. Choi, J. W. Chung and S. Y. Kwak, *ACS Appl. Mater. Interfaces*, 2014, **6**, 11118-11128.
  - 32 T. Li, J. Zhang, H. Wang, Z. Hu and Y. Yu, *ACS Appl. Mater. Interfaces*, 2013, **5**, 8968-8981.
  - 33 C. Dong, C. Yuan, X. Bai, X. Yan and Z. Peng, *RSC Advances*, 2014, **4**, 19034.
  - 34 C. Chen, J. Liu, F. Sun and J. W. Stansbury, *J. Polym. Sci. Part A: Polym. Chem.*, 2014, **52**, 2830-2840.
  - 35 Z.B. Shao, C. Deng, Y. Tan, M.J. Chen, L. Chen and Y.Z. Wang, *ACS Applied Materials & Interfaces*, 2014, **6**, 7363-7370.
  - 36 C. Yang, G. Liang, A. Gu and L. Yuan, *Ind. Eng. Chem. Res.*, 2013, **52**, 15075-15087.
  - 37 X. H. Li, Y. Z. Meng, Q. Zhu and S. C. Tjong, *Polym. Degrad. Stab.*, 2003, **81**, 157-165.
  - 38 Y.W. Yan, L. Chen, R.K. Jian, S. Kong and Y.Z. Wang, *Polym. Degrad. Stab.*, 2012, **97**, 1423-1431.
  - 39 W. H. Awad and C. A. Wilkie, *Polymer*, 2010, **51**, 2277-2285.
  - 40 X. Wang, J. Zhan, W. Xing, X. Wang, L. Song, X. Qian, B. Yu and Y. Hu, *Ind. Eng. Chem. Res.*, 2013, **52**, 5548-5555.
  - 41 X. Wang, *J. Anal. Appl. Pyrol.*, 92 (2011) 164-170, 2011, **92**, 164-170
  - 42 D. Yuan, H. Yin and X. Cai, *J. Therm. Anal. Calori.*, 2012, **111**, 1531-1537.
  - 43 Q. Tang, R. Yang and J. He, *Ind. Eng. Chem. Res.*, 2014, **53**, 9714-9720.
  - 44 K. Lu, X. Cao, Q. Liang, H. Wang, X. Cui and Y. Li, *Ind. Eng. Chem. Res.*, 2014, **53**, 8784-8792.
  - 45 X. Qian, L. Song, S. Jiang, G. Tang, W. Xing, B. Wang, Y. Hu and R. K. K. Yuen, *Ind. Eng. Chem. Res.*, 2013, **52**, 7307-7315.
  - 46 K. Täuber, F. Marsico, F. R. Wurm and B. Schartel, *Polym. Chem.*, 2014, **5**, 7042-7053.
  - 47 L. Chen, C. Ruan, R. Yang and Y.Z. Wang, *Polym. Chem.*, 2014, **5**, 3737.
  - 48 X. Han, J. Zhao, S. Liu and Y. Yuan, *RSC Advances*, 2014, **4**, 16551.
  - 49 M.J. Chen, C.R. Chen, Y. Tan, J.Q. Huang, X.L. Wang, L. Chen and Y.Z. Wang, *Ind. Eng. Chem. Res.*, 2014, **53**, 1160-1171.
  - 50 Z. B. Shao, C. Deng, Y. Tan, M. J. Chen, L. Chen and Y. Z. Wang, *ACS Appl. Mater. Interfaces*, 2014, **6**, 7363-7370.
  - 51 F. Liao, L. Zhou, Y. Ju, Y. Yang and X. Wang, *Ind. Eng. Chem. Res.*, 2014, **53**, 10015-10023.



In this work, we prepared two novel reactive-type halogen-free and UV-curable phosphorus–nitrogen–silicon synergistic flame retardants. Flame-retardant epoxy composites (FR-Ep) with different contents of PNSis were prepared from ERL4221 and cross-linked through UV-radiation. Both of the obtained flame retardants were characterized via FTIR,  $^1\text{H}$  NMR, and  $^{31}\text{P}$  NMR, and the influence of DPP-Si and PSAP on the flame-retardant properties of FR-Ep was investigated through limiting oxygen index (LOI) and vertical burning tests (UL-94) respectively. Meantime, The microstructures of the char were investigated by scanning electron microscopy (SEM), the SEM results indicated that the appearance of residual char of the FR-Eps after burning showed exactly compact and coherent, which may play an important role in the excellent thermal stability and improves flame retardancy of FR-Ep. The volatile components released of FR-Eps were investigated via TG-IR. In summary, Taking advantage of the combined benefits of phosphorus, nitrogen and silicon elements, the obtained flame retardants exhibited efficient flame retardancy and good solubility in epoxides.